The opposing roles of E2A and Id3 that orchestrate and enforce the naïve T cell fate

Masaki Miyazaki[1], **Richard R Rivera**[1], **Kazuko Miyazaki**[1], **Yin C Lin**[1], **Yasutoshi Agata**[2], and **Cornelis Murre**[1]

[1]Department of Molecular Biology University of California, San Diego La Jolla, CA92093

[2]Department of Medical Chemistry Faculty of Medicine Kyoto University

Abstract

It is established that E2A and its antagonist, Id3, modulate developmental progression at the pre-TCR receptor (pre-TCR) and TCR checkpoints. Here we demonstrate that Id3 expression is elevated beyond the pre-TCR checkpoint, remains high in naive T cells and shows a bimodal pattern in the effector/memory population. We show how E2A promotes T-lineage specification and how pre-TCR mediated signaling affects E2A genome-wide occupancy. Thymi in Id3-deficient mice exhibited aberrant development of effector/memory cells, increased CXCR5 and Bcl6 expression, T-B cell conjugates and remarkably B cell follicles. Collectively, these data show how E2A acts globally to orchestrate T-lineage development and that Id3 antagonizes E2A activity beyond the pre-TCR checkpoint to enforce the naïve T cell fate.

T-lineage cells can be defined by the expression of cell surface markers and the rearrangement of *Tcr* loci[1]. They arise from progenitors that lack the expression of the co-receptors CD4 and CD8, also named the double negative compartment (DN). The DN compartment can be further separated into four subsets characterized by the expression of CD25 and CD44. The DN1 (CD44$^+$CD25$^-$) compartment contains the T cell progenitors. The progenitors in the DN1 that express c-Kit that are named earliest T-progenitor cells (ETPs)[2]. T cell development begins at the DN2 (CD44$^+$CD25$^+$) stage, but commit to the T-cell lineage only upon differentiating into DN3 cells (CD44$^-$CD25$^+$). V-(D)J gene rearrangement is initiated at the DN2-DN3a stage. A productive *Tcrb* gene rearrangement promotes the assembly and expression of the pre-TCR complex and leads to differentiation into DN3b[3-5].

DN3b thymocytes differentiate into DN4, which in turn, progress to the ISP cell stage prior to developing into CD4+CD8+ double positive (DP) T cells[3]. At the DP stage, *Tcra* VJ rearrangement is initiated and completed. Expression of the αβ TCR is followed by interacting with auto-antigens and major histocompatibility complex antigens (MHC), a process named positive selection. Upon a productive interaction of the TCR complex with MHC, DP cells developmentally progress beyond the TCR checkpoint, to become either CD4 or CD8 single positive (SP) cells.

It is now established that a substantial fraction of developmental trajectories involves regulation by members of the helix-loop-helix (HLH) family[6]. A subset of HLH proteins consists of E-proteins, which bind the consensus E2-box site (GCAGGTGG) and function either as transcriptional activators or repressors[7]. Four E-proteins have been identified and characterized[8]. They include E12, E47, HEB and E2-2. E12 and E47 are encoded by the *E2a* locus (also known as *Tcf3*) and are generated by differential splicing of an exon encoding for either the E12 or E47 HLH domain[9]. HEB and E2-2 are related to the *E2A* gene products but diverge substantially in the N-terminal transactivation domains[7,8]. E-protein DNA binding activity is regulated by the *Id* gene products[10]. There are four Id proteins, named Id1-4. Id proteins contain a HLH dimerization domain but lack a basic region and suppress the DNA binding activities of E-proteins[11].

E-protein abundance is high in T cell progenitors where they activate *Tcrb* gene V(D)J rearrangement, induce the expression of genes encoding for proteins involved in the Notch- and pre-TCR signalling and antagonize proliferation[12,13,14,15,16]. E47 protein abundance remains high in DN4 but decrease once cells reach the ISP compartment and decline further during positive selection[17]. Id3 concentrations are elevated during β- as well as positive-selection[17,18]. High E2A abundance prevents developmental progression whereas a decline in E2A DNA binding activity promotes β- as well as positive-selection[19,20,21]. HEB enforces the TCR checkpoint and is required to promote NKT cell development[20,22]. Recent studies have demonstrated a role for the inhibitory HLH protein, Id3, in suppressing the development of Vγ1.1Vδ6.3 as well as innate-like CD8 cells[23-27]. Id3 was also shown to modulate the developmental progression of regulatory T and T_H17 cells[28].

Here we show that, using an Id3-GFP reporter strain, high abundant Id3 expression was mainly associated with a naïve T cell phenotype whereas the absence of Id3 in peripheral T cells was predominantly linked with the effector/memory population. We demonstrate at a global scale how the induction of Id3 expression at the pre-TCR checkpoint altered E2A-mediated enhancer selection to establish the αβ T cell fate. Finally, a substantial fraction of Id3-deficient thymocytes expressed a subset of genes that are closely associated with a T follicular helper (T_{FH}) phenotype, including *Cxcr5* and *Bcl6*. Taken together, these observations reveal at a global scale how E2A orchestrates T cell development whereas Id3 acts to maintain the naïve T cell fate.

RESULTS

Expression of Id3 in the thymus and peripheral splenocytes

To monitor Id3 expression in developing T-lineage cells, we inserted the coding sequence for green fluorescent protein (GFP) into the exon encoding the Id3 HLH region. The targeted allele resulted in a mutated Id3 locus, in which the expression of GFP was placed under control of regulatory elements present in the *Id3* locus (**Fig. 1a**). Mice heterozygous for the *Id3*[GFP] allele developed normally, showed normal reproductive ability, and were indistinguishable from their wild-type littermates (data not shown).

We monitored for Id3 expression by measuring GFP fluorescence in cells derived from *Id3*[GFP/+] mice. Id3-GFP expression was barely detectable in the DN3a (CD27^{low}) compartment but was substantially elevated at the DN3b (CD27^{high}) stage (**Fig. 1b**). To further evaluate the expression of Id3 in non- versus β-selected cells, DN3a and DN3b cells that either lacked or showed Id3 expression, were examined for the expression of intracellular TCRβ. Id3 expression was primarily detected in cells expressing the TCRβ chain and predominantly in large cycling DN3b cells (**Fig. 1c**). These data are consistent with the notion that Id3 expression is elevated in response to pre-TCR signalling[17]. Upon developing into the DP compartment, Id3 expression progressively increased, reaching highest abundance in positively selected CD5^{+} or CD69^{+} DP cells (**Fig. 1,d,e**). In contrast, E2A-GFP expression remained high until cells reached the resting DP compartment (**Supplementary Fig. 1**).

In the peripheral lymphoid tissues, Id3 expression remained high (**Fig. 1f**). High Id3 abundance was observed in the CD62L^{+}CD44^{lo} and CD62L^{+}CD44^{hi} compartments (**Fig. 1f**). In contrast, the CD62L^{−}CD44^{hi} compartment showed a bimodal distribution of Id3-GPF fluorescence with a substantial fraction of cells lacking Id3 expression (**Fig. 1f**). Notably, Id3-GFP expression was also absent in a small proportion of the CD4^{+}CD25^{−}IL7Rα^{hi} expressing cells and within the majority of cells expressing CD4^{+}CD25^{−}CD122^{+} (**Fig. 1g**). The largest proportion of CD4 cells in the spleen that lacked Id3-GFP expression was found in the CD44^{hi}CD122^{+} compartment. In sum, these data indicate that Id3 expression progressively is increased beyond the pre-TCR and the TCR checkpoints, remains high in naïve peripheral T cells and shows a bimodal pattern in the effector/memory compartment.

Genome-wide E2A occupancy orchestrates T-cell fate

As a first approach to determine how E2A and Id3 contribute to establish the αβ-T lineage we examined the global distribution of E2A bound sites in the DN3 and DN4 compartments. The small size of the DN3 and DN4 compartments makes it difficult to perform a genome-wide analysis of transcription factor binding sites. Thus, we utilized an approach that permits the generation of a largely uniform population of DN3 and DN4 cells. Specifically, mice deficient for Rag2 were injected with antibodies directed against CD3ε to promote developmental progression from DN3 into DN4 cells. Two days post-injection, thymocyte suspensions were prepared, analyzed for the expression of CD25 and CD44 (data not shown) and fixed using formaldehyde. Cross-linked DNA was immunoprecipitated using an E2A antibody in order to determine the dynamics of genome-wide E2A occupancy during β-

selection. Additionally, active and poised enhancer elements in the DN3 and DN4 compartments were identified using antibodies directed against monomethylated H3K4 (ref.[29]). Immunoprecipitates were examined, in parallel with genomic DNA isolated for total fixed chromatin, using deep DNA sequencing. Repetitive sequence reads were eliminated and the locations and clusters of the remaining reads were computationally identified[29,30]. We identified 939 E2A-bound sites in DN3 versus 340 DN4, indicating that the number of E2A bound sites declines substantially upon transiting through the β-selection checkpoint (**Fig. 2a**). A substantial number of E2A-bound sites (247) were shared between DN3 and DN4 but few sites that showed E2A binding were unique for the DN4 compartment (**Fig. 2a; Supplementary Fig. 2**). Thus, genome-wide E2A occupancy declines during β-selection in developing thymocytes, consistent with the induction of Id3 expression upon pre-TCR assembly.

The question arose as to whether the differences in occupancy in DN3 versus DN4 affect binding site selection. To address this issue we identified consensus-binding sites associated with E2A occupancy on the basis of statistical enrichment. As expected, the E2A consensus-binding site (CAGCTG) was ranked as the top-scoring consensus-binding site, both in the DN3 and DN4 compartments (**Fig. 2b**)[30,31]. We also identified a second consensus DNA sequence (GCAGATG) that was associated with E2A occupancy but restricted to the DN3 compartment (**Fig. 2b**). Interestingly, the GCAGATG motif has been previously identified as a Tal1/Scl recognition site[32]. In the DN3 compartments, E2A bound regions were also enriched for transcription factor motifs associated with Runx as well as ETS occupancy (**Fig. 2b**). Collectively, these data indicate that during β-selection E2A bound regions are associated with distinct sets of putative regulatory elements in the DN3 versus DN4 compartments.

The global analysis described above permitted us to examine the pattern of E2A occupancy during β-selection at a subset of genes known to play critical roles in T-lineage specification. The analysis revealed many targets predicted to be associated with E2A occupancy, including Hes1, Notch1, Notch3, Ptcra, Rag1-Rag2 and Cd3e (**Fig. 2c**)[13,16]. E2A binding at these sites was consistently associated with the E2A consensus-binding site (CAGCTG) and declined substantially upon differentiating into DN4 (**Fig. 2c**). Further inspection also revealed potential novel E2A targets, including Zap-70 (**Fig. 2d**). Zap70 expression was significantly elevated in DN4 cells[33]. Consistent with these observations we found that ZAP70 expression was initiated in CD27^{hi}DN3b cells and increased further in the DN4 and ISP cell stages (**Fig. 2e,f**). The Zap-70 locus showed substantial E2A occupancy within a putative enhancer region in the DN4 compartment, raising the possibility that Zap70 expression is regulated by E2A beyond the pre-TCR checkpoint. To test this possibility directly, we examined Zap-70 expression by intracellular staining in both Id3- and E2A-deficient thymocytes. Consistent with the binding patterns, the absence of Id3 elevated Zap70 expression whereas upon depletion of E2A, Zap70 expression declined substantially (**Fig. 2e,f**). To confirm E2A occupancy at these target loci, we performed ChIP assay using wild-type lineage-negative thymocytes, comprised primarily of DN3 cells (>82%). As described above for *Rag2*^{−/−} cells, wild-type DN3 cells, exhibited significant E2A binding to H3K4me1 islands across the examined loci (**Supplementary Fig. 3**).

Thus, the E2A proteins modulate programs of gene expression both prior and beyond the pre-TCR checkpoint. Taken together, these data reveal how the E2A proteins act in thymocyte progenitors to activate a T-lineage specific program of gene expression. Furthermore, the data indicate that upon pre-TCR expression, Id3 abundance is elevated to decrease E2A occupancy across a large spectrum of putative enhancer elements.

Id3 enforces the naïve T cell phenotype beyond the pre-TCR checkpoint

As aforementioned, previous observations have indicated multiple roles for Id3 in developing thymocytes[21,23-28]. To further evaluate the role of Id3 in thymocyte development beyond the pre-TCR checkpoint, we expanded the analysis using flow cytometry. The γδ T cell compartment was substantially increased consistent with previous observations (**Fig. 3a**)[23-26]. We also found that the expression of CD44 was substantially elevated in the DN1 compartment (**Fig. 3a**). The increase in cells that express CD44 was not caused by an expansion of T cell progenitors but rather was observed within the c-kit negative population (**Fig. 3a**). In fact, CD44 expression was detected at substantially higher abundance in virtually all thymocyte compartments beyond the pre-TCR checkpoint (**Fig. 3b**). Consistent with these data, we found E2A occupancy across the CD44 locus in DN4 but not in DN3 cells (**Supplementary Fig. 4**). The fraction of interferon-γ (IFN-γ) expressing cells was substantially elevated in CD4SP Id3-ablated cells as previously reported (**Fig. 3c**)[27]. Consistent with previous observations, we detected a substantial fraction of cells expressing PLZF but lacking NK1.1 expression (**Fig. 3d** and data not shown)[25,27]. In addition, we found that Eomes but not T-bet was aberrantly expressed in a fraction of Id3-deficient CD4SP cells (**Fig. 3d** and data not shown). Collectively, these observations indicate that Id3-deficient thymocytes aberrantly express markers that are associated with innate- and effector/memory-like phenotypes.

Aberrant development of T_{FH}-like cells in the thymus of Id3-deficient mice

As aforementioned, we observed an increase in CD44 positive cells across the entire spectrum of thymocyte compartments (**Fig. 3b**). To further evaluate the compartments that showed elevated expression of CD44, we examined Id3-deficient thymocytes for the expression of genes linked with an effector/memory phenotype including the T_{FH} related markers CXCR5. Notably, whereas as expected wild-type CD4SP cells lacked CXCR5 expression, a substantial fraction of Id3-deficient CD4SP cells expressed CXCR5 (**Fig. 4a**; top). CD4SP CXCR5$^+$ cells in the thymus of $Id3^{-/-}$ mice expressed high level of both PD-1 and ICOS, markers that are closely associated with T_{FH} cells (**Fig. 4a**, bottom). We observed a significant increase in the percentage and absolute number of CD4SP CXCR5$^+$PD-1$^+$ICOS$^+$ cells in $Id3^{-/-}$ mice (**Fig. 4a**). $Id3^{-/-}$ T_{FH}-like cells also expressed relatively abundant Ly108, a member of Slam family (Slamf6) that is required for the formation of stable T-B conjugates (**Fig. 4b**)[34]. Abnormal CXCR5 expression was already observed in $Id3^{-/-}$ DN4 cells (**Fig. 4c and Supplementary Fig. 5**). We note that abnormal ICOS and PD-1 expression was not restricted to CXCR5 expressing cells in Id3-deficient thymocytes (data not shown) and CXCR5 expressing cells were found not only in $Id3^{-/-}$ CD4SP but also in $Id3^{-/-}$ CD8SP cells (**Supplementary Fig. 6**). Collectively these data

indicate that Id3-deficient thymocytes express markers consistent with an effector/memory phenotype and that a subset of this population resembles a T_{FH} phenotype.

Since T_{FH} cells support the proliferation of B cells and germinal center formation, we examined $Id3^{-/-}$ thymi for B cell cellularity. A substantial increase in the proportion and absolute numbers of B220$^+$CXCR5$^+$ cells was observed in $Id3^{-/-}$ thymi (**Fig. 4d**). Id3-deficient thymic B cells (B220$^+$CD19$^+$) also exhibit a mature phenotype as demonstrated by the expression of CXCR5, IgM, and IgD (**Supplementary Fig. 7**). We observed increased and dispersed numbers of B220$^+$ cells throughout the thymus derived from 4-6 weeks old $Id3^{-/-}$ mice (**Fig. 4e**). Remarkably, we found that a substantial fraction of 4-6 months aged thymi exhibited B cell follicles (**Fig. 4e**). Furthermore, we detected a small but significant fraction of CD4$^+$CXCR5$^+$ population that was conjugated to B220$^+$ cells in Id3-ablated thymi (**Fig. 4f**). In contrast, $Id3^{-/-}$ CD8SP and DP cells failed to associate with B220$^+$ cells (**Fig. 4f**).

To confirm the aberrant expression of markers associated with a T_{FH}-like phenotype, we examined for the presence of Cxcr5, Slamf1 and Bcl6 transcripts in CD4SP cells using real-time PCR[35,36]. We found that whereas the quantity of Cxcr5 transcript levels was elevated, Slamf1 (CD150) abundance was reduced in Id3-deficient CD4SP cells, consistent with a T_{FH}-like phenotype (**Fig. 4g**). In addition, we observed upregulation of Slamf1 in E2A deficient immature DN cells (**Supplementary Fig. 8**). A slight increase was observed in Bcl6 transcript abundance in RNA derived from Id3-ablated CD4SP cells (**Fig. 4g**; top) [35,36]. To examine Bcl6 transcript abundance in CXCR5 expressing cells, CD44^{hi}CXCR5$^+$ CD4SP thymocytes were purified from 4-week or 4-month-old $Id3^{-/-}$ mice, and Bcl-6 transcript levels were examined and compared to those found in T_{FH} cells derived from immunized wild-type mice. Bcl-6 mRNA abundance was elevated in CXCR5$^+$CD4SP cells derived from $Id3^{-/-}$ thymi as compared to naïve wild-type CD4 T cells (**Fig. 4g**; bottom). However Bcl6 transcripts were less when compared to T_{FH} cells isolated from immunized wild-type mice (**Fig. 4g**; bottom).

Since Id3 is well known to antagonize the activity of E2A, we examined whether the T_{FH}-like phenotype relate to elevated levels of E2A DNA binding activity. As a first approach to address this question, we generated $E2A^{ff}Cd4^{Cre}Id3^{-/-}$ mice. The CD4-Cre transgene is transcribed at developmental stages beyond the pre-TCR checkpoint[37]. Cellularity in thymi derived from $E2A^{ff}CD4^{Cre}Id3^{-/-}$ mice was partially restored when compared to Id3$^{-/-}$ mice (**Fig. 5a**). IFN-γ, PLZF and Eomes expression was not detectable in $E2A^{ff}CD4^{Cre}Id3^{-/-}$ CD4SP cells (**Fig. 5b,c**). The proportion of CXCR5 and CD44 expressing cells in $Id3^{-/-}$ thymocytes was also affected by the absence of E2A (**Fig. 5d,e**). Finally, the fraction of B220$^+$CXCR5$^+$ cells was reduced in $E2A^{ff}CD4^{Cre}Id3^{-/-}$ mice (**Fig. 5f**). In sum, we conclude that E2A and Id3 modulate the expression of markers, including CXCR5 and Bcl-6, which are associated with a T_{FH}-like phenotype.

Effector/memory-like cells in the thymus of Id3-deficient mice

To further analyze the activated phenotype in thymocytes derived from Id3-deficient mice we examined $Id3^{-/-}$ thymocytes for the expression of CD122 as well as CD127[39]. Notably,

the proportion of cells expressing CD44, CD122 and CD127 was significantly elevated in Id3-deficient thymocytes, although the absolute cell number were not significantly affected (**Figs. 6a,b**).

These data bring into question as to how the absence of Id3 relates to the aberrant expression of Cxcr5, Il2rb, Icos and Pdcd1. It is conceivable that at a subset of these genes Id3 ablation elevates E2A occupancy at enhancer elements to modulate patterns gene expression within the CD4 lineage. Alternatively, higher abundance of E2A activity may act indirectly to induce the inappropriate expression of Cxcr5, Icos, Il2rb and Pdcd1. As a first approach to distinguish between these possibilities we examined enhancer elements within the Cxcr5, Icos, Il2rb and Pdcd1 loci for the presence of E2A binding sites. To identify such putative regulatory elements we re-examined genome-wide E47 occupancy as obtained by deep-DNA sequencing using an E2A^{−/−} T cell line reconstituted with forced E47 expression[30]. This analysis revealed E47 occupancy at H3K4me1 islands within the Cxcr5 and Il2rb loci (**Fig. 6c**). To examine for aberrant E2A occupancy at these sites in *Id3*^{−/−} thymocytes, CD4SP and DP cells were purified and analyzed by ChIP (**Fig. 6d**). An increase in E2A occupancy to binding sites present in putative Cxcr5 and Il2rb enhancer regions was observed. The differences in E2A occupancy were modest but we note that only a fraction of Id3-ablated CD4SP cells expressed CXCR5 and IL-2Rβ (CD122). Collectively, these data indicate that a subset of loci whose expression is modulated in Id3-deficient mice exhibit abnormally elevated E2A occupancy at putative enhancer elements, directly linking Id3 and E2A occupancy with the aberrant development of an effector/memory-like population in Id3-deficient thymocytes.

Effector/memory-like cells in the spleen of Id3-deficient mice

To determine whether *Id3*^{−/−} mice also exhibit abnormalities in the peripheral lymphoid organs we examined splenocytes derived from wild-type and Id3-ablated mice for CD44 and CD62L expression. Id3-deficient mice showed a severe reduction in the naïve CD4 compartment with a substantial increase in the fraction of CD62L^{−}CD44^{+} compartment, consistent with previous observations (**Fig. 7a**)[28]. In addition, we found that a substantial fraction of CD4 splenocytes aberrantly expressed IFN-γ as well as IL-4 upon exposure to PMA and ionomycin (**Fig. 7b**). As described for the thymus of *Id3*^{−/−} mice, a substantial fraction of CD4 splenocytes expressed CXCR5 and CD44. The CXCR5^{+}CD44^{+} compartment also exhibited high amounts of ICOS and PD-1 (**Fig. 7c**). Furthermore, *Id3*^{−/−} CXCR5^{+}CD4 T cells comparably expressed Ly108 similar to that of wild-type CXCR5^{+}CD4 T$_{FH}$ cells (**Supplementary Fig. 10**). Since T$_{FH}$ cells localize to the B cell zone we examined the distribution of CD3ε expressing cells within the context of the splenic architecture. In wild-type mice, CD3ε expressing cells were primarily detected in the T cell area (**Fig. 7d**). In contrast, Id3-ablated mice showed a substantial fraction of T-lineage cells located away from the T cell zone, whereas in *E2A*[ff]*CD4*[Cre]*Id3*^{−/−} mice a normal distribution of CD3ε expressing cells was observed throughout the spleen (**Fig. 7d and Supplementary Fig. 10**).

Consistent with the flow cytometric analysis, both CXCR5 and Slamf1 transcript levels were modulated in *Id3*^{−/−} CD4 T cells (**Fig. 7e**, top). RNA derived from *Id3*^{−/−}

CD44^{hi}CXCR5$^+$CD4$^+$ splenocytes also showed higher levels of Bcl-6 expression as compared to wild-type naïve CD4 T cells (**Fig. 7e**; bottom). A large fraction of Id3-deficient CD44^{hi} cells expressed abundant amounts of both CD127 and CD122. However, unlike the thymus we found an increase in the fraction of CD44^{hi}CD127^{lo} effector cells in the spleen (**Fig. 7f**). Furthermore, we observed a significant increase in the fraction of CD44^{hi}CD122$^+$CD127$^+$ memory-like cells in *Id3$^{-/-}$* CD4 T cells (**Fig. 7f**). Taken together, these data indicate that Id3 acts throughout T-lineage development to enforce the naïve T cell fate.

DISCUSSION

Whereas there is now ample evidence that the E2A proteins activate the expression of a large subset of target genes, including Ptcra, Hes1, Notch1, Notch3, Cd3e, Tle3, Tle5 and Tcrb, much less is known as to how the genome-wide activity of E2A is modulated. It is generally assumed that the DNA binding activity of E2A is antagonized by the induction of Id3 expression mediated by pre-TCR signalling. However, this has remained to be proven. Here we demonstrate at a global scale that E2A occupancy decreases at a large subset of putative enhancer elements. Specifically, we found that 692 bound regions were restricted to the DN3 compartments, 247 sites overlapped between the DN3 and DN4 compartments and 93 E2A bound sites were detected in the DN4 compartment. The decline in the number of E2A-bound sites at the pre-TCR checkpoint is striking and consistent with an increase in Id3-GFP expression in DN3b. Thus, upon pre-TCR mediated signaling, Id3 abundance is increased to suppress E2A occupancy at the vast majority of binding sites. We suggest that this decrease in global occupancy underpins the mechanism that promotes β-selection.

The global studies showed that the consensus DNA sequence (CAGCTG) associated with E2A occupancy is identical in two entirely different cell lineages: DN3 and pro-B cells[30]. Thus, E2A proteins recognize the same binding site in committed B- and T-cells. However, the enhancer repertoires associated with E2A binding in B versus T cells are quite distinct. E2A binding to cistromic elements is highly enriched for EBF binding sites in pro-B cells whereas DN3 cells do not show such an association. Similarly, whereas E2A binding sites are frequently associated SCL/TAL consensus-binding sites in DN3 cells, E2A bound-sites are not enriched for SCL/TAL consensus sequences in pro-B cells. Thus, whereas E2A binds to the same consensus-binding site in the B- versus T-cell lineage, E2A occupancy is associated with different enhancer repertoires in pro-B versus DN3 cells. These data indicate that it is the difference in collaborative interactions at cis-regulatory elements that underpin the mechanism by which E2A proteins promote specific programs of gene expression in distinct lineages.

The cistromic elements associated with E2A occupancy in DN3 cells are frequently enriched for RUNX as well as ETS consensus binding sites. RUNX1 binds in the DN3 compartment to sites present in the CD4 silencer and Ets-1 has been demonstrated to play an essential role in β-selection as well as allelic exclusion[41,42]. The collaborative interactions involving E2A and RUNX are of particular interest. Thus, the global analysis confirmed previous observations, identified novel targets, new participants as well as novel links between

participants and showed how pre-TCR mediated signaling, at a global and mechanistic scale, promotes developmental progression.

The data also provided new and surprising roles for Id3 in maintaining the naïve CD4 T cell fate. T_{FH} cells are not normal residents of the thymus. Thus, we are now faced with the question as to how Id3 ablation results in the development of T_{FH}-like cells in the thymus? The data indicate that a subset of genes associated with at T_{FH}-like program of gene expression, including CXCR5, is directly regulated by the E2A versus Id3 ratio. However, since only a fraction of CD4SP thymocytes express CXCR5, it seems unlikely that direct regulation by E-proteins is the only mechanism that underpins the aberrant development of T_{FH}-like cells in *Id3-/-* thymi. Rather, we suggest that the development of abnormal effector/memory cells in Id3-ablated thymocytes is, in part, a consequence of compromised TCR mediated signaling. It is now well established that Id3 acts down-stream of TCR mediated signaling[18]. Id3-deficient thymocytes show severe defects in positive selection in transgenic mouse models and develop autoimmune disease[21,44]. Thus the absence of Id3 may alter the threshold to thymic selection, resulting in the positive selection of cells that normally would be negatively selected, contributing to the aberrant activation of genes associated with an effector/memory phenotype. Of interest with regard to the defect in positive selection in *Id3*^{−/−} mice is the observation that the E2A/Id3 ratio regulates the expression of Zap70. Recent observations have indicated that altered thymic selection caused by a mutation in the Zap70 locus leads to the development of autoimmune disease[43]. It is conceivable that altered levels of components involved in TCR mediated signal strength such as ZAP-70 contribute to the defects in positive selection observed in *Id3*^{−/−} mice as well as the aberrant development of effector and/or memory-like cells. Consistent with this model are recent findings indicating that positive selection is highly sensitive to the dosage of ZAP-70 expression [45]. External factors may contribute as well to the aberrant development of T_{FH}-like cells in *Id3*^{−/−} thymocytes, as observed for the development of innate CD8-like cells[27]. In sum, we suggest that the aberrant activation of gene expression associated with an effector/memory phenotype in *Id3-/-* thymocytes is a result of aberrant E-protein activity, compromised TCR signaling and an abnormal thymic environment.

Do these data suggest that E- and Id-proteins modulate the development of follicular B and T cells in the peripheral organs? Previous observations have indicated a decrease in the number of naïve T cells in *Id3-/-* mice[28]. We have confirmed these findings but suggest that because of the lymphopenic environment in *Id3-/-* mice the defect in the naïve peripheral compartments may be caused, at least in part, by homeostatic proliferation. *E2A+/-* mice show a substantial defect in follicular B cell compartments whereas Id3-deficient mice show an increase in the number of follicular B cells[46]. Thus, the E2A/Id3 and Bcl6/CXCR5 connection might be shared between follicular B and T cells. Finally, we note that it remains to be determined as to how closely related *Id3-/-* T_{FH}-like cells observed in the spleen are to wild-type T_{FH} cells and it will be essential to ablate Id3, E2A as well as HEB in peripheral CD4 cells in order to carefully evaluate their roles in peripheral T_{FH} cell maturation.

We have previously demonstrated that Id3 expression in DP thymocytes is directly regulated by TCR mediated signaling[18]. Consistent with these data we show that Id3 expression progressively increases beyond the pre-TCR and the TCR checkpoints and remains high in

naïve peripheral T cells. However, Id3 expression in the effector/memory compartment is quite distinct. It shows a bimodal pattern of expression including a substantial fraction of the effector/memory compartments exhibiting barely detectable levels of Id3 expression. How is Id3 expression differentially regulated? We would like to suggest that it is the difference in signal strength mediated by the TCR that determines Id3 abundance. Thus, upon recognition of self-antigens in the thymus, Id3 expression becomes elevated as described previously[18]. We speculate that upon exposure to non-self antigens in the peripheral organs Id3 expression is modulated again to promote differentiation, into either the effector and/or memory cell lineages. Although still to be proven, we propose that it is the difference in Id3 abundance in the naïve versus effector and memory compartments that ultimately determines peripheral T cell fate.

METHODS

Mice

C57BL/6, *Id3*$^{gfp/+}$, E2a$^{gfp/gfp}$, *Id3*$^{-/-}$, E2a$^{-/-}$, *Rag2*$^{-/-}$, E2a^{ff}*CD4*^{cre} mice were bred and housed in specific pathogen-free conditions in accordance with the Institutional Animal Care and Use Guidelines of the University of California, San Diego.

Flow cytometry

Single cell suspensions from bone marrow, thymus and spleen were stained with the following; FITC-, PE-, APC-, APC-Cy7, Pacific Blue-, Alexa Fluor 700-, Alexa Fluor 780-, PE-Cy5.5-, PE-Cy7-, or biotin-labeled monoclonal antibodies were purchased from BD PharMingen (CD5 (53-7.3), CD122 (TM-b1), CD11c (HL3), CD44 (IM7), IL-17 TC11-18H10), CXCR5 (2G8)), eBioscience (CD8 (53-6.7), CD62L (MEL-14), CD44 (IM7), CD69 (H1.2F3), CD117 (2B8, ack45), CD127 (A7R34), B220 (RA3-6B2), Mac1 (M1/70), Gr1 (RB6-8C5), Nk1.1 (PK136), Ter119 (TER119), TCRβ (H57), TCRγδ (GL3), PD-1 (J43), ICOS (7E.17G9), IFN-γ (XMG1.2), IL-2 (JES6-5H4), IL-10 (JES5-16E3), IL-17 (17B7), Rorγt (AFKJS-9), Zap70 (1E7.2), TBR2 (Dan11mag)) or Biolegend (CD3ε (2C11), CD4 GK1.5), CD8 (53-6.7), CD25 (PC61), CD27 (LG.3A10), CD84 (mCD84.7), CXCR3 (CXCR3-173), Ly108 (13G3-19D), IL-4 (11B11) and T-bet (4B10)). Anti-PLZF antibody was purchased from Santa-Cruz (clone D9). Biotinylated antibodies were labelled with streptavidin-conjugated Qdot 665 (Invitrogen). Clone 2.4 G2 anti-CD32:CD16 (eBioscience) was used to block FcRs. Dead cells were removed from analysis and sorting by staining with propodium iodide (PI) (Sigma-Aldrich). Mouse Treg cell staining kit (eBioscience) was used for intracellular staining of PLZF, Eomes, Rorγt, T-bet and ZAP70. Samples were collected on a LSRII (BD Biosciences) and were analyzed with FlowJo software (TreeStar). Cells were sorted on a FACSAria. For intracellular staining of IFN-γ, IL-4, IL-10 and IL-17, thymocytes were first stained with biotinylated antibodies (CD4SP; TCRγδ, CD8, Mac1, B220, CD8SP; TCRγδ, CD4, Mac1 and Gr1), bound to anti-biotin-magnetic beads and depleted by AutoMACS. Negative cells were then treated with phorbol 12-myristate 13-acetate (PMA) plus ionomycin (5 h) and Golgi stop (2h). After culture, cells were stained with anti-CD4, CD8, TCRγδ, TCRβ, CD44 and CD3ε antibodies. Intracellular staining was performed with the BD Biosciences Cytofix/Cytopermkit.

Immunohistochemistry

Spleen and thymus were snap-frozen in liquid nitrogen, and stored at -80°C. Cryostat sections were cut, air-dried at 20°C for 30 min, and fixed in acetone for 10 min. Sections were incubated with the appropriate dilution of primary biotinylated Abs for 2 h followed by HRP Streptavidin (Jackson) for 30 min. 3-Amino-9-ethylcarbazole (AEC; Vector Laboratories) was used as chromogen and the slides were counterstained with Mayer's haematoxylin for 2 min.

RNA isolation and RT-PCR

Quantitative real-time RT-PCR was performed on cDNAs obtained from purified CD4 SP or splenic CD4 T cells derived from $Id3^{+/+}$ or $Id3^{-/-}$ mice. Total RNA was isolated from sorted cells using an RNeasy kit (Qiagen) and was reverse-transcribed with SuperScript III RT-PCR system (Invitrogen).

Chromatin immunoprecipitation

Chromatin was immunoprecipitated as described. Cells were fixed for 5-20 min at 20°C with 1% (wt/vol) formaldehyde, then lysed and sonicated. MACS-purified DP and CD4SP thymocytes derived from $Id3^{+/+}$ and $Id3^{-/-}$ mice were dual cross-linked with 1% formaldehyde and EGS. Nuclei were prepared, lysed and sonicated. Sonicated chromatin was immunoprecipitated with 10 μg anti-E2A (sc-349; Santa Cruz Biotechnology) and anti-H3K4me1 (ab8895; Abcam). Samples were washed, then bound chromatin was eluted and incubated overnight at 65 °C for reversal of crosslinking. Samples were next treated with RNase A and proteinase K and were purified with a PCR purification kit (Qiagen). PCR was performed using SYBR Green Master (Roche).

ChIP-Seq analysis

Chromatin was immunoprecipitated as described previously[30]. Briefly, cells were fixed with 1% formaldehyde for 5 to 20 min at 20°C and sonicated. Sonicated chromatin was immunprecipitated with 10 μg of anti-E2A (Santa Cruz Biotechnology) or 10 μg anti-H3K4me1 (ab8895) coupled to Dynal-beads. Bound chromatin was immunoprecipitated and eluted. Cross-linking was reversed by overnight incubation at 65 °C and the samples were subsequently treated with RNase A and Proteinase K. Next, samples were purified using a PCR Purification Kit (Qiagen), adapter-ligated and amplified by PCR as described (Illumina). Immunoprecipitated DNA was sized selected (150 to 250 bp) by gel electrophoresis and sequenced for 36 cycles. Reads were aligned to the mm8 assembly (NCBI Build 36) using Bowtie. Visualization was performed using custom tracks generated by the UCSC Genome browser.

DNA sequence analysis

Data was analyzed using HOMER software (http://biowhat.ucsd.edu/homer/). ChIP-Seq bound sites were identified using HOMER. Occupied sites were identified by searching for groups of tags positioned within a sliding 200 bp window. The threshold for the number of tags generating an interacting site was determined for a false discovery rate of 0.001. Furthermore, peaks were required to exhibit at least 4-fold more tags (normalized versus

total number) versus input control samples. To avoid identifying DNA elements that contain genomic duplications or non-localized occupancy, a four-fold increase in the number of tags relative to tags located within immediate genomic proximity was chosen as a threshold. In order to identify H3K4 methylated islands, the peak finding procedure was altered. The peak region was required to show 4-fold more tags (as compared to total tag count) than controls. Additionally, DNA bound elements were required to exhibit at least 4-fold more tags within a 1 kb region versus flanking 10 kb DNA regions.

Statistical Analysis

P values were calculated with the two-tailed Student's test for two group comparison as applicable with Microsoft Excel Software. The statistical significance level was 0.05.

Supplementary Material

Refer to Web version on PubMed Central for supplementary material.

ACKNOWLEDGMENTS

References

1. Kreslavsky T, Gleimer M, Garbe AI, von Boehmer H. αβ versus γδ fate choice: counting the T-cell lineage at the branch point. Immunol. Rev. 2010; 238:169–181. [PubMed: 20969592]

2. Allman D, Sambandam A, Kim S, Miller JP, Pagan A, Well D, Meraz A, Bhandoola A. Thymopoiesis independent of common lymphoid progenitors. Nat. Immunol. 2003; 4:168–174. [PubMed: 12514733]

3. Taghon T, Yui MA, Pant R, Diamond RA, Rothenberg EV. Developmental and molecular characterization of emerging beta- and gammadelta-selected pre-T cells in the adult mouse thymus. Immunity. 2006; 24:53–64. (2006). [PubMed: 16413923]

4. Yashiro-Ohtani Y, He Y, Ohtani T, Jones ME, Shestova O, Xu L, Fang TC, Chiang MY, Intlekofer AM, Blacklow SC, Zhuang Y, Pear WS. Pre-TCR signaling inactivates Notch1 transcription by antagonizing E2A. Genes Dev. 2009; 23:1665–1676. [PubMed: 19605688]

5. Carpenter AC, Bosselut R. Decision checkpoints in the thymus. Nat. Immunol. 2010; 8:666–673. [PubMed: 20644572]

6. Murre C. Developmental trajectories in early hematopoiesis. Genes Dev. 2009; 15:2366–2370. [PubMed: 19833763]

7. Zhang J, Kalkum M, Yamamura S, Chait BT, Roeder RG. E-protein silencing by the leukemogenic AML1-ETO fusion protein. Science. 2004; 305:1286–1269. [PubMed: 15333839]

8. Massari ME, Murre C. Helix-loop-helix proteins: regulators of transcription in eukaryotic organisms. Mol. Cell Biol. 2000; 18:3130–3139. [PubMed: 9584154]

9. Beck K, Peak MM, Ota T, Nemazee D, Murre C. Distinct roles for E12 and E47 in B cell specification and the sequential rearrangement of immunoglobulin light chain loci. J. Exp. Med. 2009; 206:2271–2284. [PubMed: 19752184]

10. Benezra R, Davis RL, Lockshon D, Turner DL, Weintraub H. The protein Id: a negative regulator of helix-loop-helix DNA binding proteins. Cell. 1990; 61:49–59. [PubMed: 2156629]

11. Kee BL. E and Id proteins branch out. Nat. Rev. Immunol. 2009; 9:175–184. [PubMed: 19240756]

12. Barndt RJ, Dai M, Zhuang Y. Functions of E2A/HEB heterodimers in T-cell development revealed by a dominant negative mutation of HEB. Mol. Cell. Biol. 2000; 20:6677–6685. [PubMed: 10958665]

13. Ikawa T, Kawamoto H, Goldrath AW, Murre C. E proteins and Notch signalling cooperate to promote T cell lineage specification and commitment. J. Exp. Med. 2006; 203:1329–1342. [PubMed: 16682500]

14. Herblot S, Steff AM, Hugo P, Aplan PD, Hoang T. SCL and LMO1 alter thymocyte differentiation: inhibition of E2A-HEB function and pre-T alpha chain expression. Nat. Immunol. 2000; 1:138–144. [PubMed: 11248806]

15. Agata Y, et al. Regulation of T cell receptor beta gene rearrangements and allelic exclusion by the helix-loop-helix protein, E47. Immunity. 2007; 27:871–84. [PubMed: 18093539]

16. Schwartz R, et al. Gene expression patterns define novel roles for E47 in cell cycle progression, cytokine-mediate signalling and T-lineage development. Proc. Natl. Acad. Sci. USA. 2006; 103:9976–9981. [PubMed: 16782810]

17. Engel I, Johns C, Bain G, Rivera RR, Murre C. Early thymocyte development is regulated by modulation of E2A protein activity. J. Exp. Med. 2001; 194:733–745. [PubMed: 11560990]

18. Bain G, Cravatt CB, Loomans C, Alberola-Ila J, Hedrick SM, Murre C. Regulation of the helix-loop-helix proteins, E2A and Id3, by the Ras-ERK MAPK cascade. Nat. Immunol. 2001; 2:165–171. [PubMed: 11175815]

19. Bain, et al. Thymocyte differentiation is regulated by the activity of the helix-loop-helix protein, E47. J. Exp. Med. 1999; 190:1605–1616. [PubMed: 10587351]

20. Jones ME, Zhuang Y. Acquisition of a functional TCR during T lymphocyte development is enforced by HEB and E2A transcription factors. Immunity. 2007; 6:860–868. [PubMed: 18093538]

21. Rivera RR, Johns CP, Quan J, Johnson RS, Murre C. Thymocyte selection is regulated by the helix-loop-helix inhibitor protein, Id3. Immunity. 2000; 12:17–26. [PubMed: 10661402]

22. D'Cruz LM, Knell J, Fujimoto JK, Goldrath AW. An essential role for the transcription factor HEB in thymocyte survival, Tcra rearrangement and the development of natural killer T cells. Nat. Immunol. 2010; 11:240–249. [PubMed: 20154672]

23. Ueda-Hayakawa I, Mahlios J, Zhuang Y. Id3 restricts the developmental potential of gamma delta lineage during thymopoiesis. J. Immunol. 2007; 182:5306–5316. [PubMed: 19380777]

24. Alonzo ES, et al. Development of promyelocytic zinc finger and ThPOK-expressing innate gamma delta T cells is controlled by strength of TCR signaling and Id3. J. Immunol. 2010; 184:1268–1279. [PubMed: 20038637]

25. Lee SY, Stadanlick J, Kappes DJ, Wiest DL. Towards a molecular understanding of the differential signals regulating alphabeta/gammadelta T lineage choice. Sem. Immunol. 2010; 4:237–246.

26. Verykokakis M, Boos MD, Bendelac A, Adams EJ, Pereira P, Kee BL. Inhibitor of DNA binding 3 limits development of murine slam-associated adpator protein-dependent "innate" gammadelta T cells. PLoS One. 2010; 15:e9303. [PubMed: 20174563]

27. Verykokakis M, Boos MD, Bendelac A, Kee BL. SAP protein-dependent natural killer T-like cells regulate the development of CD8(+) T cells with innate lymphocyte characteristics. Immunity. 2010; 27:203–15. [PubMed: 20674402]

28. Maruyama T, et al. Control of the differentiation of regulatory T cells and T(H)17 cells by the DNA-binding inhibitor Id3. Nat. Immunol. 2011; 12:86–95. [PubMed: 21131965]

29. Heintzman ND, et al. Distinct and predictive chromatin signatures of transcriptional promoters and enhancers in the human genome. Nature Genet. 2007; 39:311–318. [PubMed: 17277777]

30. Lin YC, et al. A global network of transcription factors, involving E2A, EBF1 and Foxo1, that orchestrates B cell fate. Nat. Immunol. 2010; 11:635–643. [PubMed: 20543837]

31. Heinz S, et al. Simple combinations of lineage-determining transcription factors prime cis-regulatory elements required for macrophage and B cell identities. Mol. Cell. 2010; 28:576–89. [PubMed: 20513432]

32. Wadman IA, et al. The LIM-only protein LMO2 is a bridging molecule assembling an erythroid, DNA binding complex which includes the TAL1, E47, GATA-1 and Ldb1/Nl1 proteins. EMBO J. 1997; 16:3145–3157. [PubMed: 9214632]

33. Palacios EH, Weiss A. Distinct roles for Syk and ZAP-70 during early thymocyte development. J. Exp. Med. 2007; 204:1703–1715. [PubMed: 17606633]

34. Cannons, et al. Optimal germinal center responses require multistage T cell: B cell adhesion process involving integrins, SLAM-associated protein, and CD84. Immunity. 2010; 32:253–265. [PubMed: 20153220]

35. Johnston RJ, et al. Bcl6 and Blimp-1 are reciprocal and antagonistic regulators of T follicular helper cell differentiation. Science. 2009; 2:1006–1010. [PubMed: 19608860]

36. Nurieva RI, Chung Y, Martinez GJ, Yang XO, Tanaka S, Matskevitch TD, Wang YH, Dong C. Bcl6 mediates the development of T follicular helper cells. Science. 2009; 325:1001–1005. [PubMed: 19628815]

37. Wolfer, et al. Inactivation of Notch1 in immature thymocytes does not perturb CD4 or CD8 T cell development. Nat. Immunol. 2001; 2:235–241. [PubMed: 11224523]

38. Weinreich MA, Odumade OA, Jameson SC, Hogquist KA. T cells expressing the transcription factor PLZF regulate the development of memory-like CD8^{+} T cells. Nat. Immunol. 2010; 11:709–716. [PubMed: 20601952]

39. Purton JF, Tan JT, Rubinstein MP, Kim DM, Sprent J, Surh CD. Antiviral CD4+ memory T cells are IL-15 dependent. J. Exp. Med. 2007; 204:951–61. [PubMed: 17420265]

40. Georgescu C, Longabaugh WJ, Scripture-Adams DD, David-Fung ES, Ui MA, Zarnegar MA, Bolouri H, Rothenberg EV. A gene regulatory network armature for T lymphocyte specification. Proc. Natl. Acad. USA. 2008; 105:20100–20105.

41. Taniuchi, et al. Differential requirements for Runx proteins in CD4 repression and epigenetic silencing during T lymphocyte differentiation. Cell. 2002; 111:621–633. [PubMed: 12464175]

42. Eyquem S, Chemin K, Fasseu M, Bories JC. The Ets-1 transcription factor is required for complete pre-T cell receptor function and allelic exclusion at the T cell receptor beta locus. Proc. Natl. Acad. USA. 2004; 44:15712–15717.

43. Sakaguchi, et al. Altered thymic T-cell selection due to a mutation of the ZAP-70 gene causes autoimmune arthritis in mice. Nature. 2003; 426:454–457. [PubMed: 14647385]

44. Li H, Dai M, Zhuang Y. A T cell intrinsic role of Id3 in a mouse model for primary Sjogren's syndrome. Immunity. 2004; 4:551–560. [PubMed: 15485632]

45. Saini M, et al. Regulation of Zap70 expression during thymocyte development enables temporal separation of CD4 and CD8 repertoire selection at different signaling thresholds. Science Signaling. 2010; 3:114, ra23.

46. Quong MW, Martensson A, Langerak AW, Rivera RR, Nemazee D, Murre C. Receptor editing and marginal zone B cell development are regulated by the helix-loop-helix protein, E2A. J. Exp. Med. 2004; 199:1101–1112. [PubMed: 15078898]
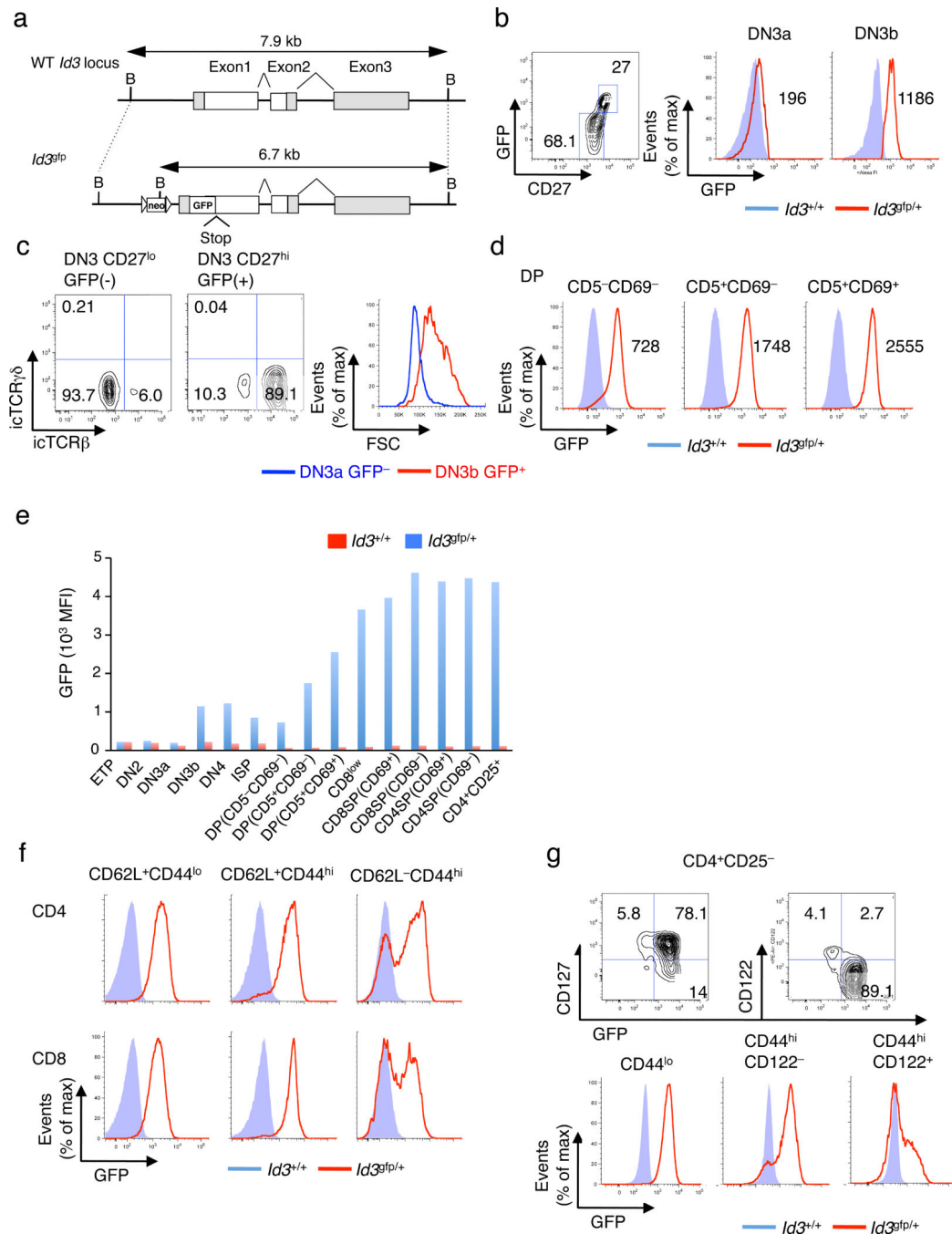
Figure 1.
Analysis of Id3 expression in thymocytes and peripheral T cells using an Id3-GFP reporter mouse strain. (**a**) Schematic representation of the *Id3* locus in which the GFP coding sequence has been inserted into the ATG initiation codon (*Id3GFP/+*). (**b**) Id3 expression is elevated beyond the pre-TCR checkpoint. Left panel shows GFP versus CD27 expression gated on the DN3 compartment. Right panel indicates GFP expression in the DN3a and DN3b (middle and right) compartments. Thymocytes were analyzed derived from both *Id3+/+* and *Id3gfp/+* mice. Numbers shown below FACS plots indicate the mean fluorescence

intensity (MFI). (**c**) Intracellular staining of TCRβ and TCRγδ expression in sorted DN3 CD27^{lo}GFP$^-$ and DN3 CD27^{hi}GFP$^+$ cells (left and middle panels). Right panel shows analysis of cell size gated on DN3a;GFP$^-$ and DN3b;GFP$^+$ cells derived from *Id3$^{gfp/+}$* mouse. (**d**) GFP expression in CD5$^-$CD69$^-$DP, CD5$^+$CD69$^-$DP, and CD5$^+$CD69$^+$ DP cells are shown. (**e**) Id3-GFP expression plotted as MFI at different stages of thymocyte development. (**f**) GFP expression was monitored in CD62L$^+$CD44^{lo}, CD62L$^+$CD44^{hi} and CD62L$^-$CD44^{hi} cells gated on the CD4$^+$(CD8$^+$) CD3$^+$TCRβ$^+$TCRγδ$^-$ isolated from *Id3$^{+/+}$* and *Id3$^{gfp/+}$* splenocytes. (**g**) Flow cytometric analyses of Id3-GFP versus CD127 and GFP versus CD122 expression are shown. Top panels show cells gated on the CD25$^-$CD4$^+$ compartment. Bottom panels indicate Id3-GFP expression in the CD44^{lo}, CD44^{hi}CD122$^-$ or CD44^{hi}CD122$^+$ cells isolated from *Id3$^{+/+}$* and *Id3$^{gfp/+}$* spleen.
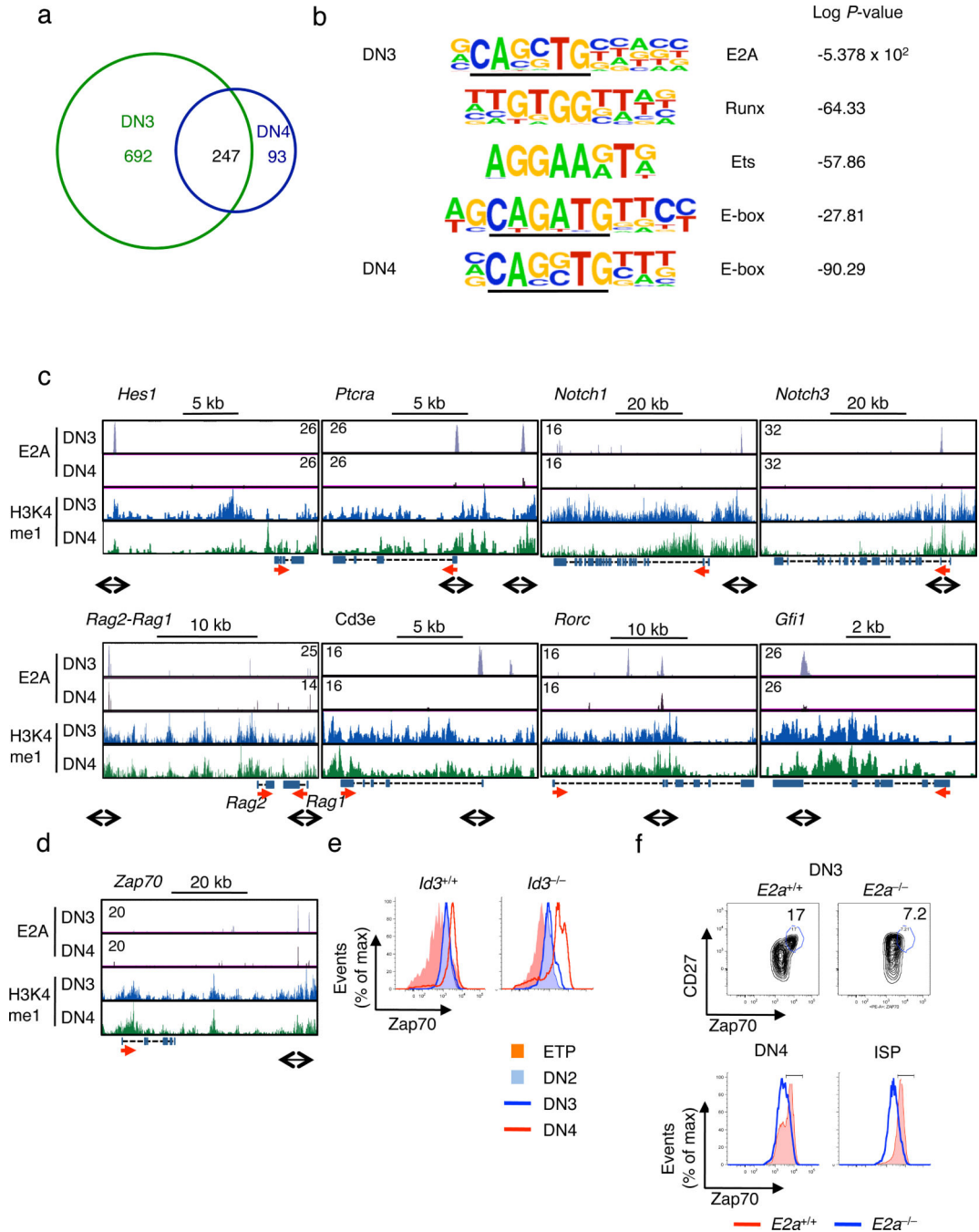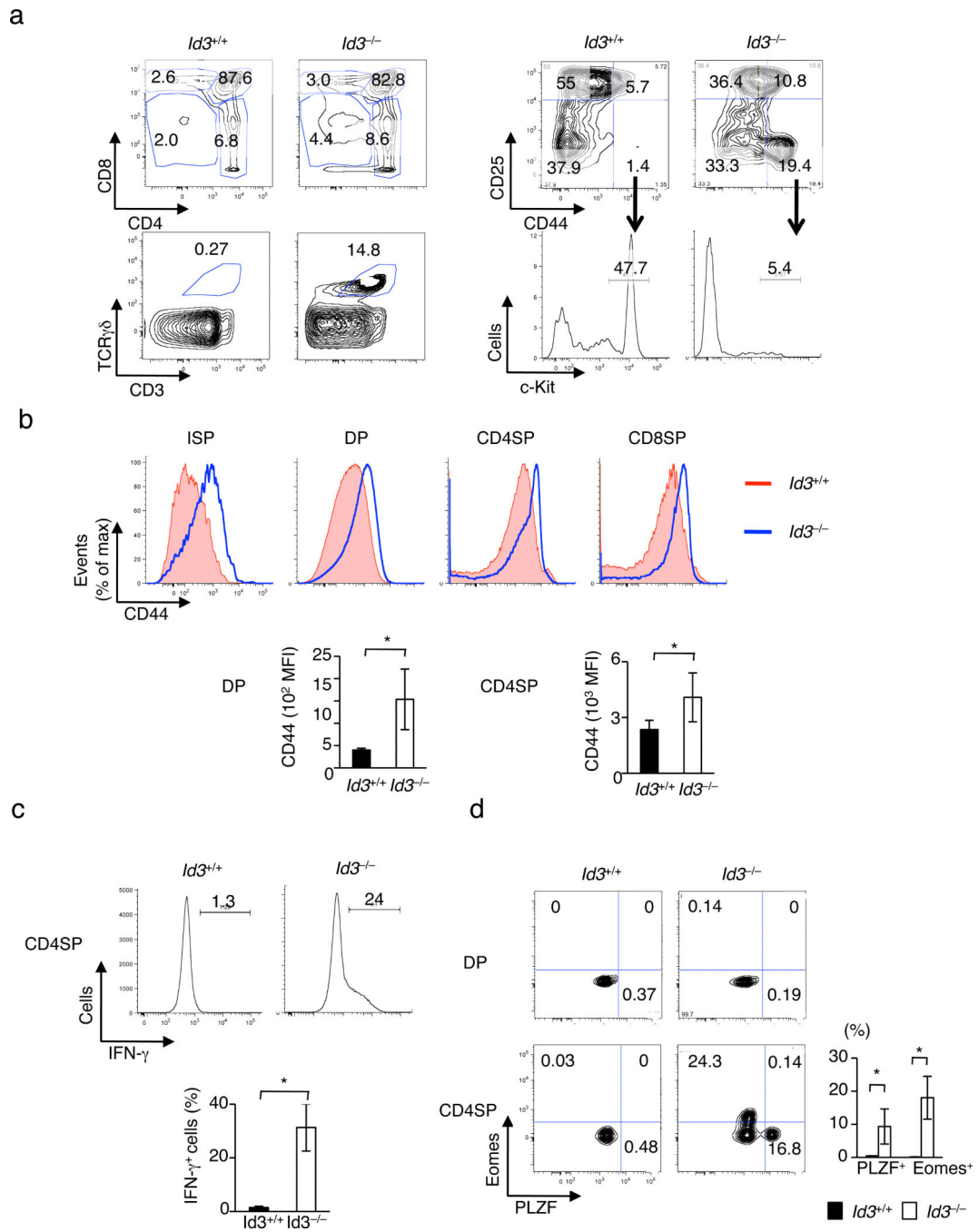
Figure 2.
Global E2A occupancy declines during β-selection. Genome-wide E2A occupancy and patterns of H3K4 mono-methylation were examined in thymocytes isolated from either untreated *Rag2*^{−/−} mice (DN3) or *Rag2*^{−/−} mice injected with anti-CD3ε antibody (DN4). (**a**) Venn diagram displaying the distribution of E2A binding sites in DN3 versus DN4. (**b**) Cis-regulatory sequences associated with E2A occupancy in DN3 and DN4, identified by comparing enriched peaks to randomly selected genomic DNA sequences. Letter size directly relates to nucleotide frequency. *P* values are shown and indicate enrichment for a

given motif as compared to randomly selected regions. (**c**) E2A occupancy and patterns of H3K4me1 across the Hes1, Ptcra, Notch1, Notch3, Rag2/1, Cd3e, Rorc and Gfi1 loci in the DN3 and DN4 compartments. E2A occupancy in DN3 is shown in gray versus black for the DN4 compartment. H3K4me1 is indicated in blue in DN3 versus green in DN4. (**d**) E2A occupancy and patterns of H3K4me1 across the Zap70 locus. (**e**) Expression of Zap70 in wild-type and Id3-deficient DN1-4 thymocyte compartments. (**f**) Expression of Zap70 and CD27 in day 16.5 dpc fetal wild-type and E2A-deficient DN3 (top) and DN4 as well as ISP (bottom) thymocytes.

Figure 3.
Id3 acts to maintain the naïve T cell fate. (**a**) Upper left panel shows CD4 versus CD8 expression gated on the γδ- population derived from wild-type and $Id3^{-/-}$ thymocytes. Lower left panels show high proportion of γδ T cells within the entire thymocyte population. Upper right panel indicates the Lineage-negative compartments. Lower right panel shows c-Kit expression in the DN1 compartment derived from wild-type and $Id3^{-/-}$ thymocytes. (**b**) Flow cytometric analyses of CD44 expression in ISP, DP, CD4SP ($CD4^+CD8^-TCR\beta^{hi}CD3\epsilon^{hi}$) and or CD8SP ($CD4^-CD8^+TCR\beta^{hi}CD3\epsilon^{hi}$) compartments

derived from wild-type (red) and *Id3*^{−/−} (blue) mice. Graphs show the MFI of CD44 expression in DP and CD4SP thymocytes. Data represent the mean ± SD analyzed in four mice. *, $P < 0.05$ (Student's *t* test). (**c**) Intracellular staining for IFN-γ expression in gated CD4SP (CD3ε⁺TCRγδ⁻ TCRβ⁺CD4⁺CD8⁻) thymocytes. Percentages of IFN-γ⁺ cells are shown. Data are representative of three independent experiments. Data represent the mean ± SD from three mice. *, $P < 0.05$ (Student's *t* test). (**d**) Representative flow cytometric analyses of PLZF versus Eomes expression in DP (upper) and CD4SP (lower) thymocyte compartments. Thymocytes were gated on the TCRγδ⁻ population isolated from 4-6 weeks old *Id3*^{+/+} and *Id3*^{−/−} mice. Data represent the mean ± SD from four mice. *, $P < 0.05$ (Student's *t* test).
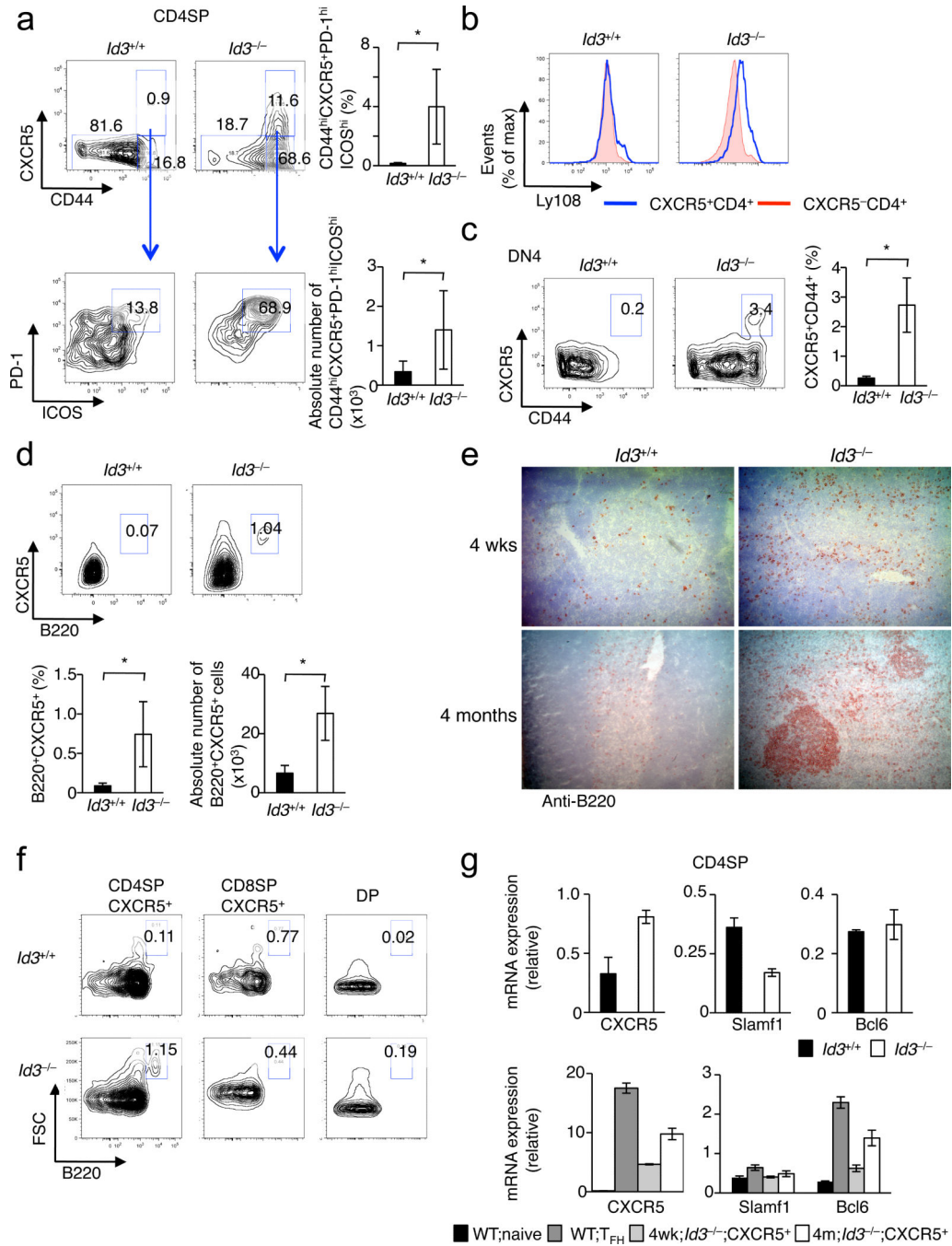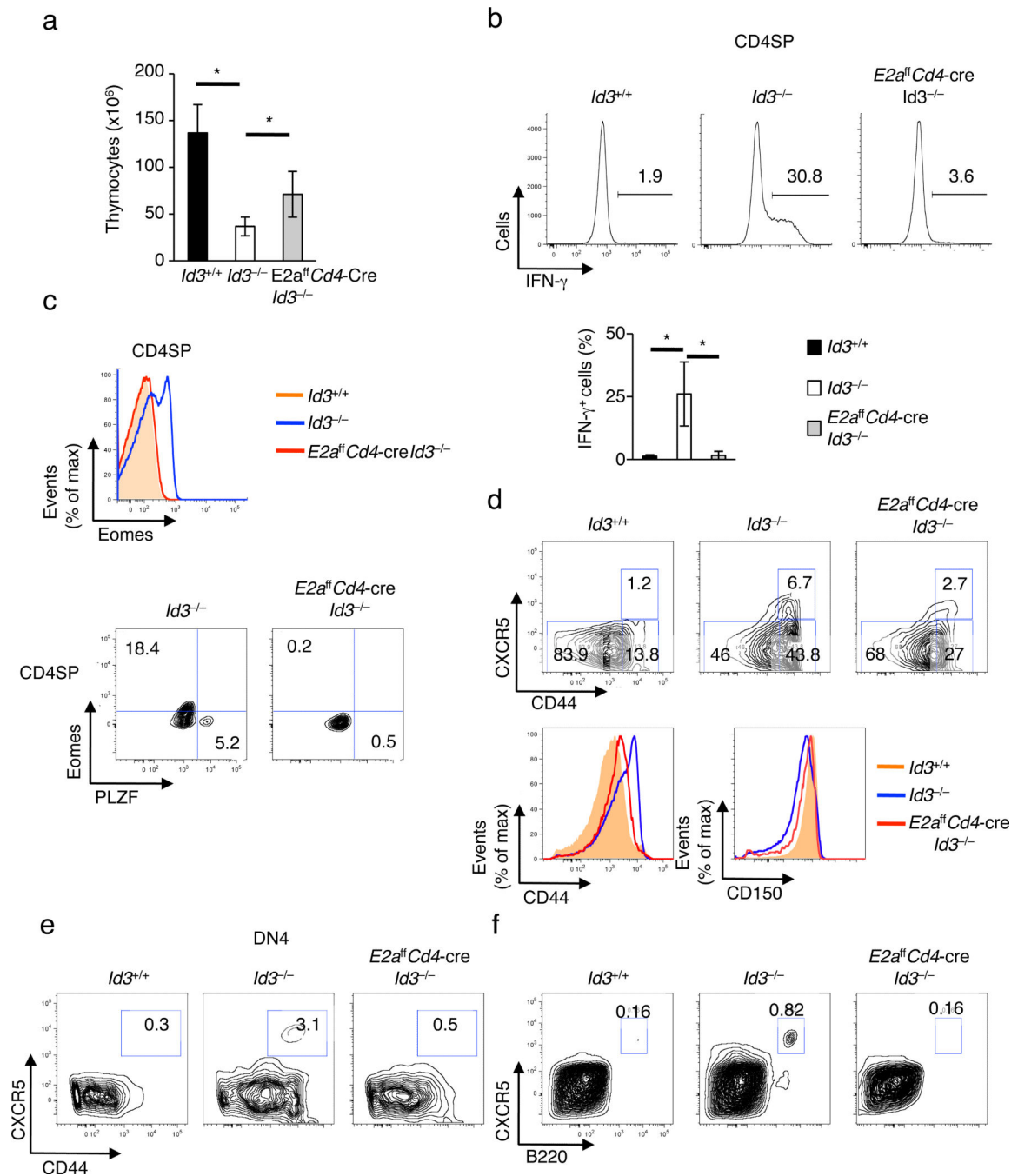
Figure 4.
Aberrant development of T_FH-like cells in $Id3^{-/-}$ thymi. (**a**) Upper panels indicate expression of CD44 and CXCR5 gated on the $CD3\epsilon^{hi}TCR\gamma\delta^-TCR\beta^{hi}CD4^+CD8^-$ compartment. Lower panels show PD-1 versus ICOS expression gated on the $CD44^{hi}CXCR5^+CD4SP$ compartments. Percent $CD44^{hi}CXCR5^+PD-1^{hi}ICOS^{hi}$ of CD4SP thymocytes (top) and its absolute number (bottom) are shown. Data represents the mean ± SD derived from analyzing four mice. *, $P < 0.05$ (Student's t test). (**b**) Ly108(Slamf6) expression in the $CXCR5^-CD4SP$ and $CXCR5^+CD4SP$ compartments. (**c**) Flow cytometric

analysis of CD44 and CXCR5 expression gated on the lineage-negative CD25⁻c-Kit⁻(DN4) compartments of wild-type and $Id3^{-/-}$ mice. Percent CXCR5⁺CD44^{hi} cells of DN4 thymocytes are shown. Data represent the mean ± SD from four mice. *, $P < 0.05$(Student's t test). (**d**) Flow cytometric analysis of B220 versus CXCR5 expression on total thymocyte population is shown. Percent B220⁺CXCR5⁺ cells of total thymocytes (bottom left) and absolute cell numbers (bottom right) are indicated. Data represent the mean ± SD from five mice. *, $P < 0.05$(Student's t test). (**e**) Immunostaining of 4-week- (upper) and 4-month-old (lower) wild-type and $Id3^{-/-}$ thymi with antibodies directed against B220. Data are representative of ten (4w) to twelve (4m) mice. 8 of 12 aged $Id3^{-/-}$ mice showed several B cell follicles in three sections of thymi. (**f**) Cells were analyzed by flow cytometry for the expression of B220 and FSC on gated CD44^{hi}CXCR5⁺CD4SP, CD44^{hi}CXCR5⁺CD8SP and DP thymocytes derived from $Id3^{+/+}$ or $Id3^{-/-}$ mice. (**g**) Cxcr5, Slamf1(CD150) and Bcl-6 transcripts in CD4SP thymocytes (top panel) and in sorted Cxcr5⁺ cells (bottom panel). Transcript levels were normalized to Hprt transcript levels. Bottom panel; wild-type naïve CD4⁺CD62L^{hi}CD44^{lo} cells isolated from unimmunized wild-type mouse spleen, wild-type T$_{FH}$ CD4⁺CD44^{hi}CXCR5⁺ cells derived from wild-type mice 10 d after immunization, and CD4⁺CD8⁻TCRβ^{hi}CD44^{hi}CXCR5⁺ cells isolated from unimmunized 4-week-old or 4-month-old $Id3^{-/-}$ thymi.

Figure 5.
Id3 acts to enforce the naïve T cell fate by suppression of intrinsic E2A activity. (**a**) Absolute thymocyte numbers in 4-6 week-old *Id3*^{+/+}, *Id3*^{−/−} and *E2a*[ff]*CD4*[cr];*Id3*^{−/−} mice are shown. Data represent the mean ± SD from six mice. *, $P < 0.05$ (Student's *t* test). (**b**) Expression of IFN-γ on gated CD4SP (CD3ε^{+}TCRγδ^{−}TCRβ^{+}CD4^{+}CD8^{−}) thymocytes using intracellular staining. Data are representative of three independent experiments. (**c**) Flow cytometric analyses of Eomes expression in CD4SP thymocytes derived from 4-week-old *Id3*^{+/+}, *Id3*^{−/−}, and *E2a*[ff]*CD4*[cre]*Id3*^{−/−} mice (top). PLZF versus Eomes expression in CD4SP

from *Id3*$^{-/-}$ and *E2A*^{ff}*Cd4*^{cre}*Id3*$^{-/-}$ mice is indicated (bottom). Data were derived from two independent experiments. (**d**) Flow cytometric analysis of CD44 versus CXCR5 expression (top), CD44 and CD150 expression (bottom) in CD4SP thymocytes. (**e**) Aberrant expression of CXCR5 in the DN4 compartment of Id3-deficient mice requires E2A activity. Flow cytometric analysis of CD44 versus CXCR5 expression on DN4 thymocytes is shown in thymocytes derived from *Id3*$^{+/+}$, *Id3*$^{-/-}$ and *E2A*^{ff}*Cd4*^{cre}*Id3*$^{-/-}$ mice. (**f**) Increased B cell cellularity in *Id3*$^{-/-}$ thymi requires intrinsic activity of E2A in the CD4 cell-lineage. Flow cytometric analysis of B220 versus CXCR5 expression on total thymocytes is shown for *Id3*$^{+/+}$, *Id3*$^{-/-}$ and *E2A*^{ff}*Cd4*^{cre}*Id3*$^{-/-}$ mice.
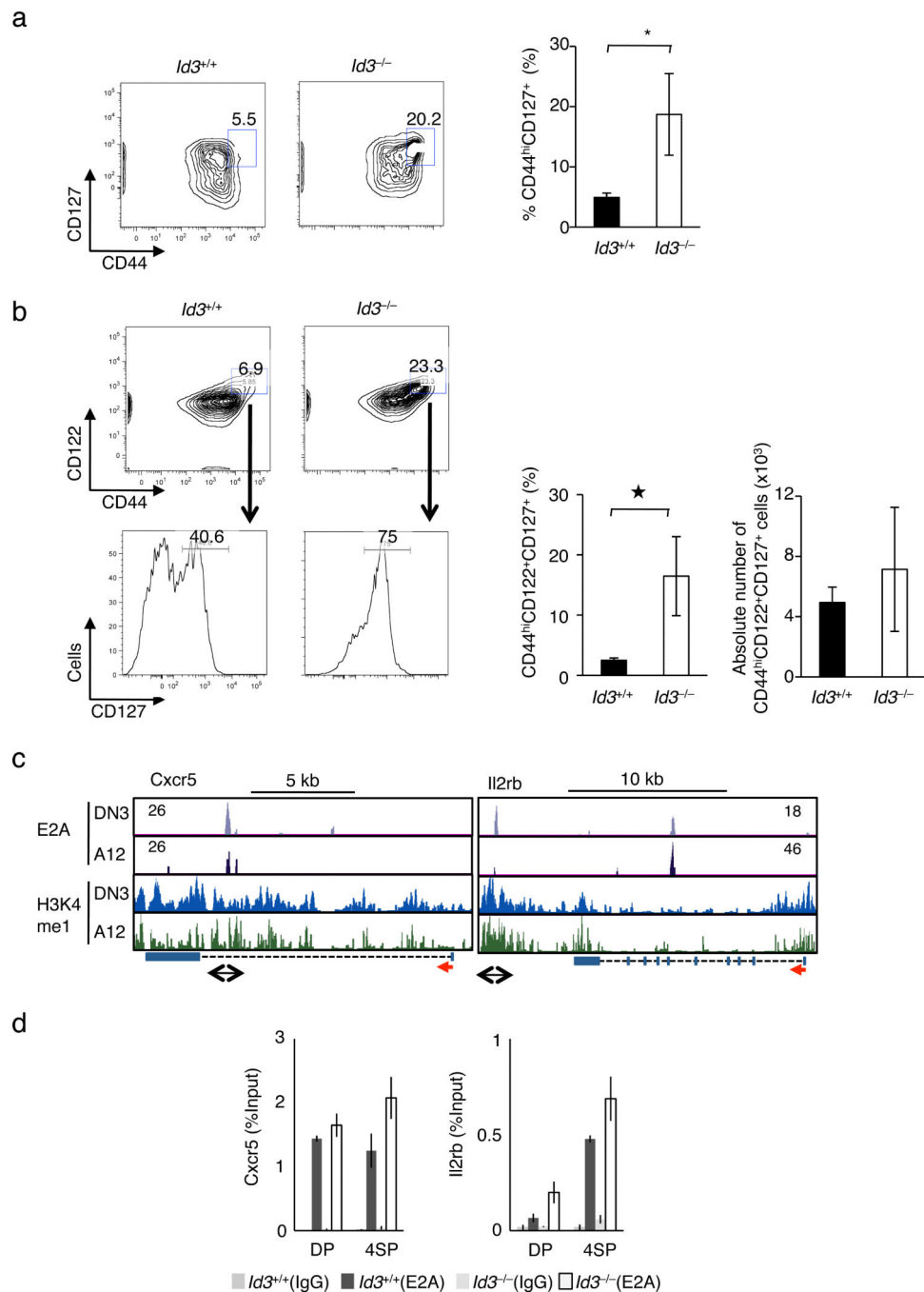
Figure 6.
Effector/memory-like CD4 T cells in the thymus of $Id3^{-/-}$ mice. (**a**) A substantial proportion of $Id3^{-/-}$ CD4 SP thymocytes express high levels of CD127 and CD44. (**b**) The fraction of $CD44^{hi}CD122^+CD127^+$ CD4SP cells is significantly increased in $Id3^{-/-}$ thymocytes. CD127 expression was gated on the $CD44^{hi}CD122^+$ CD4SP thymocytes are indicated (lower panel). Percentages of $CD44^{hi}CD127^+$ cells and $CD44^{hi}CD122^+CD127^+$ cells within the CD4SP compartment are shown. Absolute cell numbers of $CD44^{hi}CD122^+CD127^+$ cells are shown (lower right). Data represent the mean ± SD from three mice. *, $P < 0.05$ (Student's t test).

(**c**) E2A occupancy and H3K4me1 islands across the Cxcr5 and Il2rb loci in DN3 and the E47 reconstituted A12 T cell line are shown. E2A occupancy observed within the DN3 compartment is shown in gray. E2A occupancy detected within the E47 reconstituted A12 cell line is shown in black. H3K4me1 islands in DN3 cells are shown in blue. H3K4me1 islands in E47 reconstituted A12 cells are shown in green. Black arrows show the position for each of the individual PCR amplicons used for the ChIP assays as described below. (**d**) Increased E2A occupancy at putative enhancers located within the Cxcr5 and Il2rb loci in Id3-deficient thymocytes. DP and CD4SP thymocytes were purified from *Id3*^{+/+} or *Id3*^{−/−} mice and analyzed by ChIP for E2A occupancy. Real-time PCR reactions were carried out using primers for each amplicon.
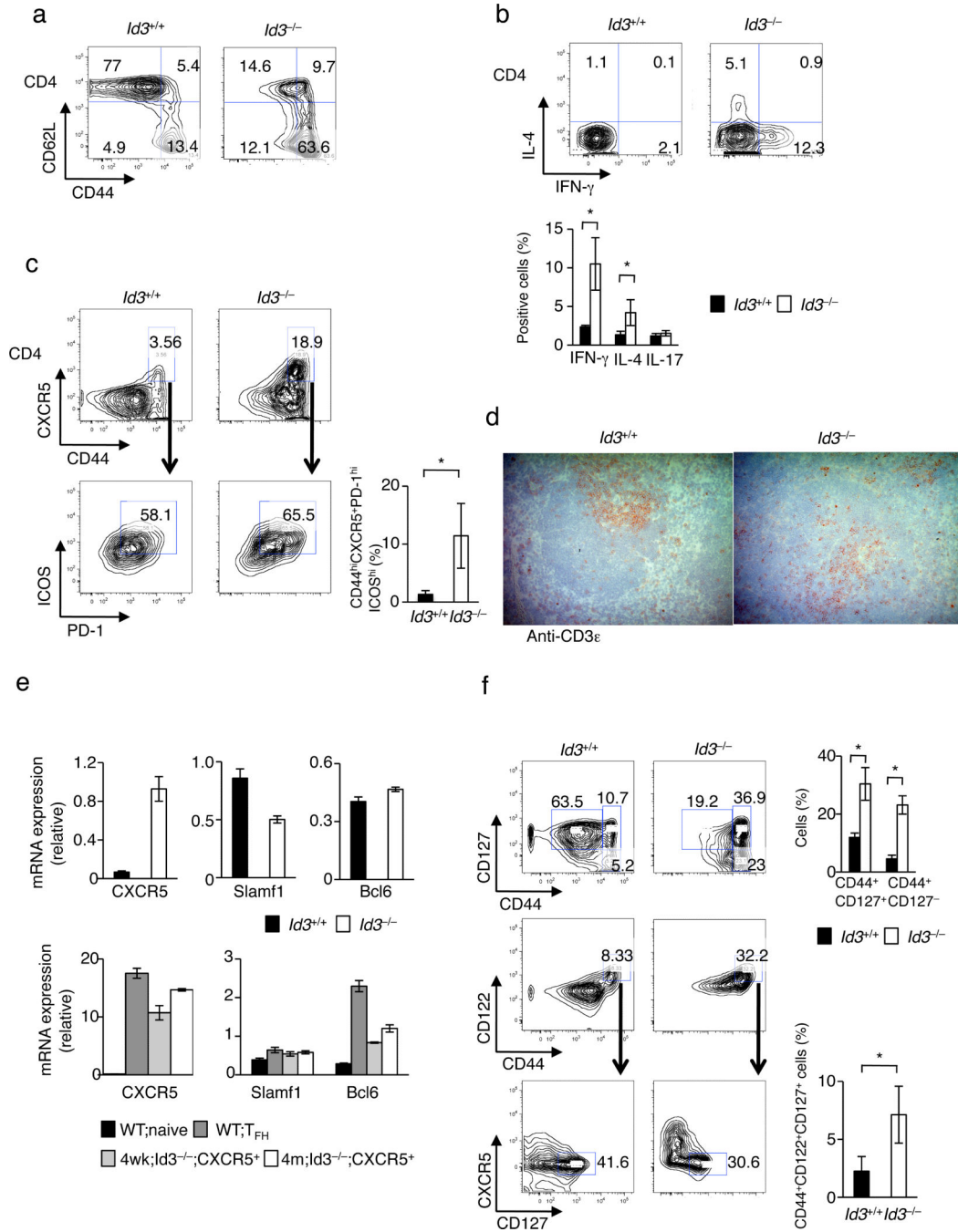
Figure 7.
Abnormal effector/memory and T$_{FH}$-like compartments in Id3-deficient spleen. (**a**) Representative flow cytometric analyses are shown for CD62L versus CD44 expression gated on CD3ε$^+$TCRγδ$^-$TCRβ$^+$CD4$^+$ splenocytes derived from 6-week-old *Id3$^{+/+}$* and *Id3$^{-/-}$* mice. (**b**) Aberrant IFN-γ and IL-4 expression in CD3ε$^+$TCRγδ$^-$TCRβ$^+$CD4$^+$ T cells isolated from 4-week-old *Id3$^{+/+}$* or *Id3$^{-/-}$* spleen. Data represent the mean ± SD derived from three mice. *, $P < 0.05$(Student's *t* test). (**c**) T$_{FH}$-like cells in Id3-deficient mice. Representative flow cytometric analyses showing CD44 versus CXCR5 expression gated on

$CD3\varepsilon^+TCR\gamma\delta^-TCR\beta^+CD4^+$(CD4) splenocytes (top) and of PD-1 versus ICOS expression gated on $CXCR5^+CD44^{high}$ CD4 T cells (middle). Data represent the mean ± SD from five mice. *, $P < 0.05$(Student's t test). (**d**) Representative immunostaining of spleen with anti-CD3ε antibody (x200). (**e**) Quantitative real-time RT-PCR analyses in $CD4^+$ T cells (top) and $CXCR5^+$ cells sorted from $Id3^{+/+}$ or $Id3^{-/-}$ spleen. Bottom panel; wild-type naïve ($CD4^+CD62L^{hi}CD44^{lo}$) from unimmunized wild-type mouse spleen, wild-type T_{FH}($CD4^+CD44^{hi}CXCR5^+$) from wild-type mice 10 days after immunization, and $CD4^+CD8^-TCR\beta^{hi}CD44^{hi}CXCR5^+$ cells from unimmunized 4-week-old or 4-month-old $Id3^{-/-}$ spleen. (**f**) Flow cytometric analyses of CD44 versus CD127, CD44 versus CD122 expression gated on CD4($TCR\gamma\delta^-TCR\beta^+CD3\varepsilon^+CD4^+$) are shown. Bottom panel indicates CD127 versus CXCR5 expression gated on the $CD44^{hi}CD122^+$ CD4 T cells derived from 4-week-old $Id3^{+/+}$ or $Id3^{-/-}$ spleen. Data represent the mean ± SD from three mice. *, $P < 0.05$ (Student's t test).